DOI: 10.1002/chem.200902668

Multifunctional Magnetic Materials Obtained by Insertion of a Spin-Crossover Fe^{III} Complex into Bimetallic Oxalate-Based Ferromagnets

Miguel Clemente-León,*[a, b] Eugenio Coronado,*[a] Maurici López-Jordà,[a] Guillermo Mínguez Espallargas,[a] Alejandra Soriano-Portillo,[a] and João C. Waerenborgh[c]

Abstract: The syntheses, structures and magnetic properties of the compounds of formula $[Fe^{III}(sal_2\text{-trien})][Mn^{II}Cr^{III}(ox)_3]\cdot CH_2Cl_2$ (**1**; H_2sal_2-trien = *N*,*N*′-disalicylidenetriethylenetetramine, ox = oxalate), $[Fe^{III}(sal_2\text{-trien})][Mn^{II}Cr^{III}(ox)_3]\cdot CH_3OH$ (**2**), $[In^{III}(sal_2\text{-trien})][Mn^{II}Cr^{III}(ox)_3]\cdot 0.25\,H_2O\cdot 0.25\,CH_3OH\cdot 0.25\,CH_3CN$ (**3**), and $[In^{III}(sal_2\text{-trien})][Mn^{II}Cr^{III}(ox)_3]\cdot CH_3NO_2\cdot 0.5\,H_2O$ (**4**) are reported. The structure of **1** presents a 2D honeycomb anionic layer formed by Mn^{II} and Cr^{III} ions linked through oxalate ligands and a cationic layer of $[Fe(sal_2\text{-trien})]^+$ complexes intercalated between the 2D oxalate network. The structures of **2**, **3**, and **4** present a 3D achiral anionic network formed by Mn^{II} and Cr^{III} ions linked through oxalate ligands with $[Fe(sal_2\text{-trien})]^+$ or $[In(sal_2\text{-trien})]^+$ complexes and solvent molecules intercalated within the 3D oxalate network. The magnetic properties and Mössbauer spectroscopy of **1** and **2** indicate that these compounds undergo a long-range ferromagnetic ordering at around 5 K and a spin crossover of the intercalated $[Fe(sal_2\text{-trien})]^+$ complexes above 130 K, which is complete in the case of **1**. The magnetic properties of the compounds **3** and **4** confirm the ferromagnetic ordering of the bimetallic oxalate network.

Keywords: coordination chemistry · iron · magnetic properties · Moessbauer spectroscopy · spin crossover

Introduction

One of the most exciting developments in molecular magnetism is the preparation of multifunctional compounds. The versatility of molecular chemistry makes possible the design of new molecule-based materials that combine two (or more) physical properties of interest. Thus, a wise choice of the constituent molecules could allow the appearance in the same compound of an unusual combination of physical properties, or even a mutual interplay—synergy—of the properties involved. A suitable approach to obtaining such materials is the so-called hybrid approach in which two-network solids are constructed through the self-assembly of two different molecular fragments (organic, inorganic, or organometallic), with each network furnishing the solid with distinct properties.[1]

Bimetallic oxalate-bridged complexes of formula $A[M^{II}M^{III}(ox)_3]$ (M^{III} = Cr, Fe, Ru, V, Mn; M^{II} = Mn, Fe, Co, Ni, Cu, Zn; ox = oxalate; A = cation) have provided many examples of hybrid magnets. These bimetallic salts are most often composed of polymeric 2D anionic networks, which furnish the cooperative magnetic properties (ferro-, ferri-, or canted antiferromagnetism),[2] and a bulky charge-compensating molecular cation, which templates the network formation. In these compounds, the cooperative magnetism of the oxalate network can coexist with the electronic properties provided by the cationic molecular lattice. Some illustrative examples of this concept are provided by the use of paramagnetic decamethylferrocenium[3] or organic radical cations,[4] photochromic molecules,[5] nonlinear optical (NLO)-active molecules,[6] organic π-electron donors,[7] and chiral

[a] Dr. M. Clemente-León, Prof. E. Coronado, M. López-Jordà, Dr. G. Mínguez Espallargas, Dr. A. Soriano-Portillo
Instituto de Ciencia Molecular, Universidad de Valencia
Polígono de la Coma s/n, 46980 Paterna (Spain)
Fax: (+34) 963543273
E-mail: miguel.clemente@uv.es
eugenio.coronado@uv.es

[b] Dr. M. Clemente-León
Fundació General de la Universitat de València (FGUV)

[c] Dr. J. C. Waerenborgh
Dept. Quimica, Instituto Tecnológico e Nuclear/CFMC-UL
2686-953 Sacavém (Portugal)

Supporting information for this article is available on the WWW under http://dx.doi.org/10.1002/chem.200902668.

cations,[8] which lead to the formation of magnetic multilayers, photochromic magnets, ferromagnetic molecular metals, or chiral magnets. More recently, the magnetochiral dichroic effect has been observed for the first time on a chiral magnet in enantiopure 2D oxalate-based magnets prepared by Train et al.[9] Other magnetic networks, different from the 2D honeycomb-like network, can also be obtained depending on the nature of the templating cation (size, shape, and charge) with dimensionalities ranging from 0D to 3D.[10] The most extensive one is represented by the family of 3D chiral structures in which the chirality of a templating cation of the type $[Z^{II}(bpy)_3]^{2+}$ (Z^{II} = Fe, Co, Ni, Ru; bpy = 2,2′-bipyridine) induces the building blocks to adopt a homochiral configuration,[11] which provides an opportunity to obtain chiral magnets.[11e,12] In addition, the hybrid character of these series also leads to examples in which the two sublattices are magnetic.[11d]

In this context, spin-crossover cations are particularly suitable to prepare multifunctional magnetic materials since they represent one of the best examples of molecular bistability. This may open a way to design switching magnets in which the magnetic ordering of the oxalate network could be tuned, thus taking advantage of the possibility of inducing the spin-crossover phenomenon by applying an external stimuli such as light or pressure. However, this challenging goal requires first the preparation of hybrid materials formed by a magnetic network and a spin-crossover complex.

The first example of the insertion of spin-crossover cations into oxalate networks was reported by Decurtins et al. in a compound of formula $[Co(bpy)_3][LiCr(ox)_3]$.[13] In that case, the insertion of a Co^{II} complex into a 3D oxalate-based network resulted in the observation of spin crossover in the Co^{II} sublattice. However, the compound did not show coexistence of spin crossover and magnetic ordering since the oxalate network was paramagnetic. More recently, our group reported the insertion of the Fe^{II} spin-crossover complex $[Fe(bpp)_2]^{2+}$ (bpp = 2,6-bis(pyrazol-3-yl)pyridine) into a ferromagnetic achiral 3D oxalate-based network, $[Fe(bpp)_2][MnCr(ox)_3]\cdot bpp\cdot CH_3OH$,[14] although spin crossover was not observed as most Fe^{II} complexes remained in the low-spin (LS) state throughout the entire temperature range. The coexistence of a spin crossover and magnetic ordering has successfully been obtained very recently by insertion of Fe^{III} complexes in homometallic oxalate layers.[15] As a result, the compound $[\{Fe^{III}(sal_2\text{-trien})\}_2][Mn^{II}_2(ox)_3]\cdot 4H_2O\cdot C_3H_7NO$ (sal_2-trien = hexadentate ligand; see Scheme 1) formed by homometallic Mn^{II} oxalate layers and $[Fe(sal_2\text{-trien})]^+$ cations behaves as a weak ferromagnet below a critical temperature (T_c) of 8.1 K and exhibits at the same time a gradual spin crossover of half of the intercalated $[Fe(sal_2\text{-trien})]^+$ complexes from 300 to 80 K. In this compound, however, the two properties seem to be independent since the change in the spin state of the inserted $[Fe(sal_2\text{-trien})]^+$ cations after desolvation does not produce important changes in the magnetic ordering of the homometallic oxalate network.

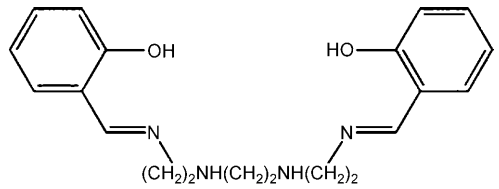

Scheme 1. H_2sal_2-trien.

In view of this first result, we have explored the insertion of the $[Fe(sal_2\text{-trien})]^+$ complex into bimetallic oxalate anionic networks. This approach has several advantages with respect to the previous one. On one hand, the use of bimetallic oxalate networks can give rise to ferro- or ferrimagnetism instead of weak ferromagnetism due to a spin canting in the antiferromagnetic state. On the other hand, the possibility of inserting the spin crossover complex into a 3D lattice could improve the effect of the spin crossover on the magnetic ordering of the oxalate network since the 3D oxalate networks are much more sensitive to small structural and size changes of the inserted cation than the 2D oxalate networks.[11f]

In this work we report the preparation and structural and magnetic characterization of the compounds $[Fe^{III}(sal_2\text{-trien})][Mn^{II}Cr^{III}(ox)_3]\cdot CH_2Cl_2$ (**1**), which presents a 2D oxalate-based anionic network, and $[Fe^{III}(sal_2\text{-trien})][Mn^{II}Cr^{III}(ox)_3]\cdot CH_3OH$ (**2**), $[In^{III}(sal_2\text{-trien})][Mn^{II}Cr^{III}(ox)_3]\cdot 0.25H_2O\cdot 0.25CH_3OH\cdot 0.25CH_3CN$ (**3**), and $[In^{III}(sal_2\text{-trien})][Mn^{II}Cr^{III}(ox)_3]\cdot CH_3NO_2\cdot 0.5H_2O$ (**4**), which present an achiral 3D oxalate-based anionic network. The compounds containing the diamagnetic $[In(sal_2\text{-trien})]^+$ complex have been studied as reference compounds.

Results and Discussion

Synthesis: The method used to prepare this family of compounds is analogous to that used to prepare the chiral oxalate 2D compound of formula $[(S)\text{-}\{PhCH(CH_3)N(CH_3)_3\}][Mn(CH_3CN)_{2/3}Cr(ox)_3]\cdot CH_3CN\cdot(solvate)$.[8] It is based on the use of $Ag_3[Cr(ox)_3]$ to avoid the presence of alkali ions in the structure. It consists of the slow diffusion of a solution containing the precursors of the oxalate network, Mn^{2+} and $[Cr(ox)_3]^{3-}$ ions, in methanol, into a solution of $[M(sal_2\text{-trien})]^+$ (M^{III} = Fe or In) in different solvents. The use of different solvents to dissolve the $[M(sal_2\text{-trien})]^+$ complex gives rise to different structures. Thus, **1** is obtained by using CH_2Cl_2, **2** and **3** by using CH_3CN, and **4** by using CH_3NO_2. The composition of these crystals, checked by microanalysis, shows in all cases a M/Mn/Cr ratio of 1:1:1. Furthermore, crystals of **1** show the presence of Cl from CH_2Cl_2 in a ratio 2:1 with respect to Mn, Cr, and Fe. It has not been possible to obtain the crystal structure of the 2D oxalate network with the $[In(sal_2\text{-trien})]^+$ cation dissolved in dichloromethane. Due to this, we have tried with other solvents such as CH_3NO_2, but this has resulted in a new compound, **4**, that presents a 3D oxalate network slightly different to that of **2**

and **3**. The crystal structures of the four compounds have been solved by single-crystal X-ray diffraction. Unit cells of several crystals obtained in the same diffusion tube have been measured by single-crystal X-ray diffraction and give similar results in all cases. This excludes the possibility of crystallization of the different structures by using the same solvent mixture. Attempts to obtain analogous compounds with other paramagnetic M^{2+} ions (M = Ni, Fe, Co, and Cu), or with other M^{III} ions (M^{III} = Fe) in the place of Cr^{III} have been unsuccessful.

Structure of $[Fe^{III}(sal_2\text{-trien})][Mn^{II}Cr^{III}(ox)_3]\cdot CH_2Cl_2$ (1): The structure of this compound is formed by anionic sheets in the *bc* plane of formula $[MnCr(ox)_3]^-$ with interlamellar $[Fe(sal_2\text{-trien})]^+$ cations and dichloromethane solvent molecules (Figure 1). The anionic layer is formed by an extended

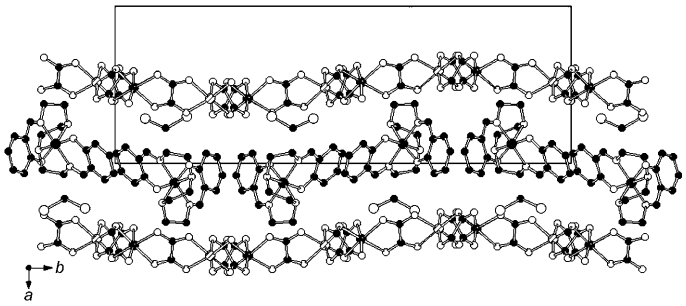

Figure 1. Projection on the *ab* plane of the structure of **1** (for clarity, neighboring atoms that correspond to disordered Mn/Cr have been assigned for Mn and Cr separately). Hydrogen atoms have been omitted for clarity.

network with Mn^{II} and Cr^{III} ions linked through oxalate bridges. It presents the well-known 2D honeycomb structure. It is formed by oxalate ligands connecting Mn^{II} with Cr^{III} ions in such a way that each Mn^{II} is surrounded by three neighboring Cr^{III} and vice versa (Figure 2). The neighboring metal centers of these layers present alternated chirality as is usual for this type of network. There are two metals that are crystallographically independent with M–O bond lengths lying between 2.061(3) and 2.107(3) Å. These bond lengths are intermediate between the ones expected for Cr^{III}–O and Mn^{II}–O. Therefore, it is not possible to distinguish between the two metals in this structure. Mean metal–metal distances between adjacent centers are in the range 5.3941(13)–5.4432(13) Å. These distances are similar to those found in other 2D oxalate networks reported in the literature[2,3] and shorter than those found in 3D systems.[11,13] The distance between metal ions of different layers is 11.6440(2) Å, which is higher than those found in other oxalate-based 2D compounds with decamethylferrocenium or alkylammonium cations (9.2–9.7 Å)[2,3] but lower than those of the $[\{Fe^{III}(sal_2\text{-trien})\}_2][Mn^{II}_2(ox)_3]\cdot 4H_2O\cdot C_3H_7NO$ compound (17.489(7) Å) in which a double layer of cations is necessary to compensate for the higher charge of the $[Mn^{II}_2(ox)_3]^{2-}$ anionic layer with respect to the $[M^{II}M^{III}(ox)_3]^-$ anionic layer.[15] These anionic layers are stacked one over the other in an *AA*… fashion. The Mn^{II} and Cr^{III} ions and oxalate ligands do not form a perfect 2D layer, as there is a certain amount of undulation of the inorganic layer (see Figure 1). The presence of ethylene groups from $[Fe(sal_2\text{-trien})]^+$ that extend alternatively above and below the layer of inserted $[Fe(sal_2\text{-trien})]^+$ complexes could be responsible for this effect. Finally, the minimum distance between the metallic ions from the oxalate network and the Fe atoms is 6.3795(9) Å.

The space between the oxalate layers is occupied by one crystallographically independent $[Fe(sal_2\text{-trien})]^+$ complex and one dichloromethane molecule (Figures 1 and 2). The

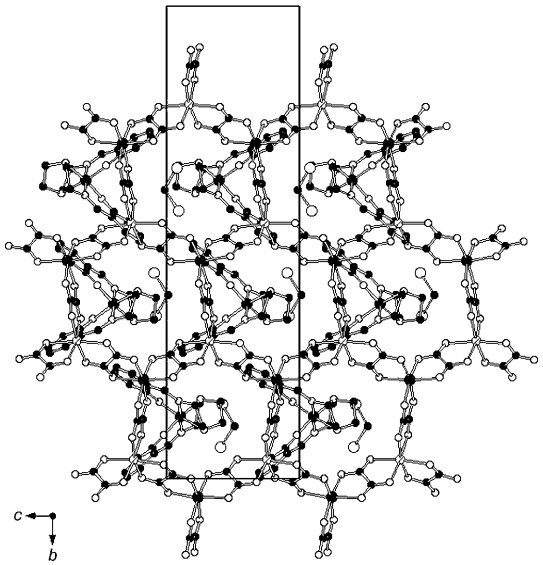

Figure 2. Projection on the *bc* plane of the structure of **1** (for clarity, neighboring atoms that correspond to disordered Mn/Cr have been assigned for Mn and Cr separately). Hydrogen atoms have been omitted for clarity.

$[Fe(sal_2\text{-trien})]^+$ cations lie with their longer axis parallel to the oxalate layers. They form double chains running along the *c* axis (Figure 1 and Figure 1SS in the Supporting Information) in which $[Fe(sal_2\text{-trien})]^+$ complexes are connected through C–H···π and N–H···π interactions.[16] Only one of the two phenoxy rings of sal_2-trien, which is placed in the internal part of the double chain, is involved in these C–H···π and N–H···π interactions with two adjacent $[Fe(sal_2\text{-trien})]^+$ complexes that belong to the same chain. These are edge-to-face interactions with a shortest distance of 3.592(7) Å between C4 and C1 of neighboring rings and 3.356(6) Å between C4 and N3 of neighboring rings (Figure 1SS in the Supporting Information). Furthermore, the phenoxy rings from $[Fe(sal_2\text{-trien})]^+$ complexes that belong to different double chains that are not involved in these interactions present short contacts with O atoms from the oxalate network ($d_{C16–O14}$ = 3.384(6) Å). Finally, there are short contacts between C atoms from ethylene groups of sal_2-trien and the oxalate ligands ($d_{C10–O13}$ = 3.152(6) Å). The average Fe–N and Fe–O bond lengths in $[Fe(sal_2\text{-trien})]^+$ complexes are

1.989(4) and 1.866(3) Å, respectively. These values are in the range of those obtained for other low-spin $[Fe(sal_2\text{-trien})]^+$ compounds[17] and are in full agreement with the magnetic measurements and Mössbauer spectroscopy (see below), which indicate that all Fe are LS at 180 K (the temperature at which the crystal structure has been determined). On the other hand, the dichloromethane molecules occupy the holes situated in between the $[Fe(sal_2\text{-trien})]^+$ cations and the oxalate network. They are placed alternatively above and below the layer formed by $[Fe(sal_2\text{-trien})]^+$ cations. They present short contacts with oxalate ligands ($d_{Cl1–O10}=3.258(3)$ Å and $d_{Cl2–O12}=2.979(3)$ Å).

Structure of $[Fe^{III}(sal_2\text{-trien})][Mn^{II}Cr^{III}(ox)_3]\cdot CH_3OH$ (2): The structure of **2** is formed by an anionic 3D polymeric oxalate-bridged bimetallic network with $[Fe(sal_2\text{-trien})]^+$ cations and solvent molecules occupying the cavities (Figure 3).

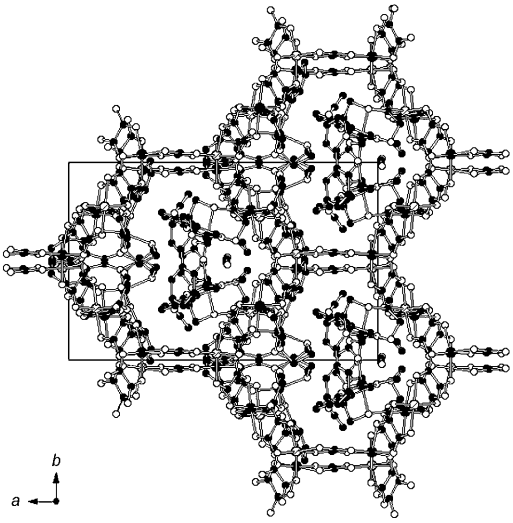

Figure 3. Projection on the *ab* plane of the structure of **2** (for clarity, neighboring atoms that correspond to disordered Mn/Cr have been assigned for Mn and Cr separately). Hydrogen atoms have been omitted for clarity.

This anionic polymeric structure is formed by bis-chelating oxalate ligands that connect Mn^{II} and Cr^{III} ions in such a way that each Mn^{II} is surrounded by three Cr^{III} and vice versa, thus building ten-membered rings in a (10,3) topology. In contrast to typical chiral structures exhibited by the oxalate-based 3D network, compound **2** possesses metal centers of both chiralities. In fact, **2** crystallizes in the acentric *Cc* space group. A similar achiral 3D oxalate network has been found in the compound of formula $[Fe(bpp)_2][\{MnCr(ox)_3\}_2]\cdot bpp\cdot CH_3OH$ that crystallizes in the centrosymmetric $P2_1/n$ space group.[14] The (10,3) decagon rings perpendicular to the *c* axis are formed by metal centers with the same chirality (see Figure 3). Two of these neighboring metal rings, which are linked through two oxalate ligands, present opposite chirality (see Figure 4). Projection of the oxalate network on the *ac* plane is almost identical to that of the chiral 3D oxalate network in the *ab*, *bc*, or *ac* planes

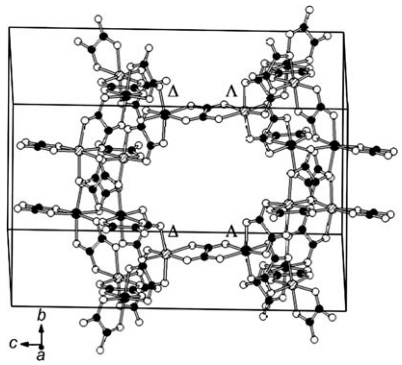

Figure 4. Two neighboring ten-membered rings of the oxalate network of **2** of opposite chirality connected through two oxalate ligands along the *c* direction (for clarity, neighboring atoms that correspond to disordered Mn/Cr have been assigned for Mn and Cr separately). Hydrogen atoms have been omitted for clarity.

(see Figure 5). However, projection on the *bc* or *ab* planes (see Figures 3 and 4) is different as a result of the different chirality of the neighboring (10,3) decagon rings. Thus, in

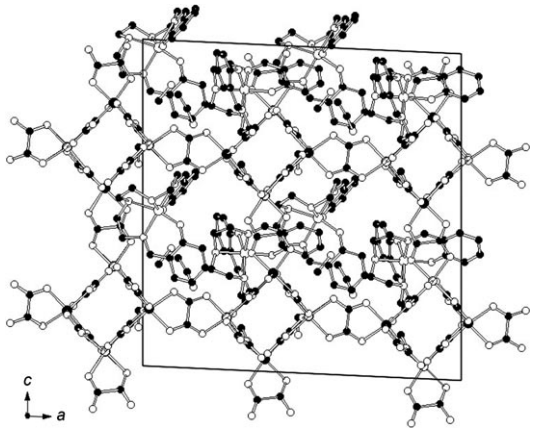

Figure 5. Projection on the *ac* plane of the structure of **2** (for clarity, neighboring atoms that correspond to disordered Mn/Cr have been assigned for Mn and Cr separately). Hydrogen atoms have been omitted for clarity.

the *ab* projection an eclipsed disposition of the neighboring oxalate rings is observed as a result of the heterochiral oxalate junctions among them (see Figure 3). This anionic network contains four metals that are crystallographically independent with M–O bond lengths lying between 2.004(14) and 2.141(13) Å. Again, these bond lengths are intermediate between the ones expected for Cr^{III}–O and Mn^{II}–O and hence it is not possible to distinguish between the two metals in this structure. Metal–metal distances between adjacent centers are in the range 5.396(3)–5.408(3) Å. These metal–metal distances are significantly shorter than those exhibited by the 3D chiral structures. For instance, the Mn–Cr distance in $[Ir(ppy)_2(bpy)][MnCr(ox)_3]\cdot 0.5H_2O$ is 5.503 Å.[11f] These metal–metal distances are shorter than those found for compound **1**, although it is important to

note that the crystal structure of compound **2** was determined at lower temperature (120 versus 180 K). In addition, the minimum distance between the metallic ions from the oxalate network and the Fe atoms is also shorter than in compound **1**. Thus, a value of 5.905(4) Å is obtained between Mn4/Cr4 and Fe1.

$[Fe(sal_2\text{-trien})]^+$ complexes and solvent molecules are intercalated in the holes described by this 3D oxalate network. There are two crystallographically independent $[Fe(sal_2\text{-trien})]^+$ complexes ([Fe1] and [Fe2]) and disordered methanol. The phenoxy rings from two neighboring crystallographically independent $[Fe(sal_2\text{-trien})]^+$ complexes present edge-to-face interactions with a shortest distance of 3.46(12) Å between C19 and C26 of neighboring rings. Furthermore, the [Fe1] complex presents hydrogen bonds through the NH groups with one disordered methanol molecule and one oxalate ligand ($d_{N3\cdots O3M}=3.11(2)$ and $d_{N2\cdots O24}=3.100(18)$ Å) and short contacts with oxalate ligands ($d_{C14-O19}=3.21(2)$ and $d_{C19-O22}=3.137(16)$ Å), whereas the [Fe2] complex forms hydrogen bonds with two disordered methanol molecules ($d_{N6\cdots O2M}=3.15(3)$ and $d_{O4\cdots O3M}=2.94(3)$ Å) and presents short contacts with oxalate ligands from the oxalate network ($d_{C29-O12}=3.05(3)$ Å). The average Fe–N and Fe–O bond lengths are 2.042(17) and 1.891(13) Å in [Fe1] complexes and 2.15(2) and 1.877(15) Å in [Fe2] complexes. These values are higher than those found in **1** and close to those obtained for other high-spin (HS) $[Fe(sal_2\text{-trien})]^+$ compounds. We have to take into account that magnetic measurements and Mössbauer spectroscopy (see below) indicates that around 28% of Fe is LS at 120 K (the temperature at which the crystal structure has been determined).

Interestingly, the use of the same templating cation in different solvents has afforded different structures. This finding is very unusual for this type of oxalate compound. The few examples in the literature in which that occurs involve either a change in the coordination mode of the oxalate ligand, or the presence of solvent molecules that complete the coordination of the metals from the oxalate network.[10k,l,18] In our case, the two different structures—a 2D and an achiral 3D oxalate network—present bis-chelating oxalate ligands that connect M^{II} and M^{III} ions. To our knowledge, this is a novel feature in this type of compound. A possible explanation may be related to the flexibility of $[Fe(sal_2\text{-trien})]^+$ cation. This complex presents two phenoxy arms projecting from the same face of the molecule.[17] The relative orientation of these arms differs notably in different compounds. Therefore, a different configuration of the phenoxy rings may have a different templating effect on the oxalate network, thus giving rise to different structures. Indeed, the configuration of $[Fe(sal_2\text{-trien})]^+$ cations in the structures of **1** and **2** confirms this point. The dihedral angles (α) between the least-squares planes of the two phenoxy rings have very different values in the 2D or 3D structures presented in this paper. Thus, $\alpha=71.65(13)°$ is present in **1**, whereas $\alpha=120.13(67)°$ ([Fe1] complex) and $\alpha=103.02(75)°$ ([Fe2] complex) are present in **2**. Whereas in the 2D compound the two phenoxy rings are clearly below 90°, the ideal value for an octahedral complex, the opposite behavior is observed in the 3D compound for the two crystallographically independent $[Fe(sal_2\text{-trien})]^+$ cations, which present α higher than 90°. Such a difference may be induced by the different solvent mixture used to dissolve the $[Fe(sal_2\text{-trien})]^+$ cations in the two compounds.

It is also possible to relate this configuration to the magnetic behavior of the $[Fe(sal_2\text{-trien})]^+$ complexes in the two compounds. Pritchard et al. have shown that there is a correlation between the disposition of the two phenoxy groups and the spin state of $[Fe(sal_2\text{-trien})]^+$ salts.[17] All $[Fe(sal_2\text{-trien})]^+$ compounds with LS state adopt a configuration with an α angle of 61.8–73.6°, whereas those presenting a HS state are much more structurally variable. They conclude that compounds presenting a low α angle, which is the preferred configuration for the LS state, can undergo a spin crossover. On the contrary, those presenting high α angles remain in the HS state, as the structural changes needed to adopt a LS state prevent the spin crossover from occurring. This is confirmed for the two compounds presented in this paper. Thus, in compound **1**, which shows a clear spin crossover (see below), $\alpha=71.65(13)°$, whereas in compound **2**, which remains mostly in the HS state throughout the entire temperature range, α values of 120.13(67) and 103.02(75)° are observed.

Structure of $[In^{III}(sal_2\text{-trien})][Mn^{II}Cr^{III}(ox)_3]\cdot 0.25\,H_2O\cdot 0.25\,CH_3OH\cdot 0.25\,CH_3CN$ (3): The structure of **3** resembles that of **2** with $[In(sal_2\text{-trien})]^+$ cations in the place of $[Fe(sal_2\text{-trien})]^+$ (see Figures 2SS, 3SS, and 4SS in the Supporting Information). The bimetallic oxalate 3D network is similar to that of **2**. It is formed by four metals that are crystallographically independent with M–O bond lengths that lie between 2.050(6) and 2.103(6) Å. Again, it is not possible to distinguish between Mn or Cr in this structure. Metal–metal distances between adjacent centers are in the range 5.3545(14)–5.4157(14) Å. The cavities of the oxalate network are occupied by two crystallographically independent $[In(sal_2\text{-trien})]^+$ complexes ([In1] and [In2]), and disordered water, methanol, and acetonitrile molecules. The disposition of the solvent molecules and $[In(sal_2\text{-trien})]^+$ differs with respect to that of **2**. In this case, the complex [In1] forms hydrogen bonds with one methanol molecule ($d_{N7\cdots O1M}=3.084(16)$ Å) and one water molecule ($d_{O50\cdots O1W}=3.038(13)$ Å), and has at the same time a short contact with an oxalate ligand ($d_{N7-O2}=3.269(13)$ Å) as well as C–H···π and N–H···π interactions with the neighboring [In2]. Apart from this short interaction between the two crystallographically independent complexes, [In2] presents one hydrogen bond with one water molecule ($d_{N2\cdots O1W}=3.033(10)$ Å) and two short interactions with an oxalate ligand ($d_{N3-O11}=3.199(7)$ and $d_{N3-O12}=3.122(7)$ Å). Dihedral angles between the phenoxy rings of [In1] and [In2] are, respectively, 120.22(52) and 102.96(60)°, similar to those found for $[Fe(sal_2\text{-trien})]^+$ complexes in compound **2**.

Structure of $[In^{III}(sal_2\text{-trien})][Mn^{II}Cr^{III}(ox)_3]\cdot CH_3NO_2\cdot 0.5H_2O$ (4): Compound **4** crystallizes in the acentric orthorhombic space group $Pna2_1$, which contains metal centers of both chiralities. It is formed by an anionic 3D polymeric oxalate-bridged bimetallic network similar to that of **2** and **3**. The cavities of this 3D network are occupied by the $[In(sal_2\text{-trien})]^+$ cations and nitromethane and water solvent molecules (Figure 6). In contrast to **2** and **3**, it is possible to

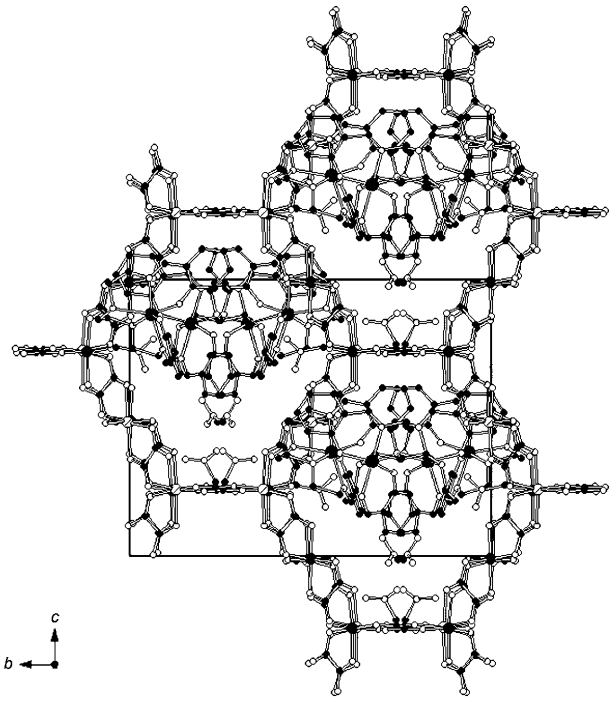

Figure 6. Projection on the *bc* plane of the structure of **4**. Hydrogen atoms have been omitted for clarity.

distinguish between Mn and Cr ions of this oxalate network. Thus, there are two crystallographically independent Mn ions (Mn1 and Mn2) with Mn–O bond lengths that lie between 2.151(6) and 2.196(6) Å and two crystallographically independent Cr ions (Cr1 and Cr2) with Cr–O bond lengths that lie between 1.957(6) and 1.988(6) Å. These are typical Cr^{III}–O and Mn^{II}–O distances similar to those found in other oxalate networks. Metal–metal distances between adjacent centers are in the range 5.3795(17)–5.4342(18) Å. These metal–metal distances are slightly shorter than those exhibited by **3** measured at the same temperature. This shortening may have some consequences on the magnetic properties (see below).

The (10,3) decagon rings formed by metal centers with the same chirality are in this case perpendicular to the *a* axis (Figure 6). Two of these neighboring metal rings, which are linked through two oxalate ligands, present opposite chirality as in the structure of **2** and **3** (see Figure 5SS in the Supporting Information). Projection of the oxalate network on the *ab* plane is almost identical to that of the chiral 3D oxalate network in the *ab*, *bc*, or *ac* planes (see Figure 6SS), whereas projections on the *bc* or *ac* planes (see Figure 6 and Figure 5SS in the Supporting Information) are different as a result of the different chirality of the neighboring (10,3) decagon rings, as observed for **2** and **3**. In this case, the eclipsed disposition of the neighboring rings is observed in the *bc* projection view (see Figure 6). In contrast to compounds **2** and **3**, which crystallize in a monoclinic space group, the eclipsed disposition of the rings is almost complete as a result of the higher symmetry of the space group of compound **4**.

The disposition of $[In(sal_2\text{-trien})]^+$ complexes and solvent molecules intercalated in the holes of this 3D oxalate network differs from that of **2** and **3**. There are two crystallographically independent $[In(sal_2\text{-trien})]^+$ complexes ([In1] and [In2]), one nitromethane molecule, and disordered nitromethane and water molecules. [In1] presents short contacts with the oxalate ligands through one of the two phenoxy rings ($d_{C14–O16}=2.924(11)$ and $d_{C15–O16}=3.168(11)$ Å). [In1] presents short contacts with two neighboring [In2] complexes. There are two types of short contacts. The first one is between the phenoxy ring of [In1] and one of the ethylene groups of [In2] ($d_{C19–C31}=3.280(18)$ and $d_{C19–N7}=3.237(15)$ Å). The second one is between one NH from [In1] and atoms from the phenoxy ring of [In2] ($d_{N3–C39}=3.218(11)$ and $d_{N3–C40}=3.294(11)$ Å). These are edge-to-face interactions. [In2] also presents short contacts with the oxalate ligands through one of the two phenoxy rings ($d_{C39–C55}=3.310(12)$ and $d_{C39–O28}=3.154(11)$ Å). Furthermore, the imine C linked to this phenoxy ring (C34) presents a short contact with another oxalate ligand ($d_{C34–O17}=2.901(12)$ Å). [In2] is also connected to two neighboring [In1] complexes through the short contacts mentioned above. The absence of methanol molecules in this structure could induce shorter contacts between neighboring $[M(sal_2\text{-trien})]^+$ complexes than those observed in compounds **2** or **3**. We have to take into account that methanol molecules of **2** and **3** are linked to sal_2-trien ligands through hydrogen bonds. Dihedral angles between the phenoxy rings of [In1] and [In2] are, respectively, 114.84(46) and 96.59(38)°.

Magnetic properties of 1: The thermal dependence of the product of the molar magnetic susceptibility with temperature (χT) of **1** is shown in Figure 7. χT shows a constant value of 10.0 emu K mol^{-1} from 400 to 350 K. This value is approximately equal to the sum of the expected contributions for the isolated paramagnetic ions with the Fe^{III} spin-crossover complex in a HS state. χT decreases gradually from 350 to 165 K as temperature decreases, with a more abrupt decrease below 300 K. The χT value at 165 K is 7.2 emu K mol^{-1}. This value of χT is consistent with the Mössbauer data that suggest that Fe^{III} is 94% LS at this temperature. Therefore, in this range of temperatures a full HS→LS spin conversion of the Fe^{III} complex takes place. At lower temperatures, there is an increase of χT that is very sharp below 50 K. This indicates the presence of ferromagnetic interactions between neighboring Mn^{II}–Cr^{III} magnetic ions and suggests the onset of long-range ferromagnetic ordering, as observed for other M^{II}–Cr^{III} 2D oxalate net-

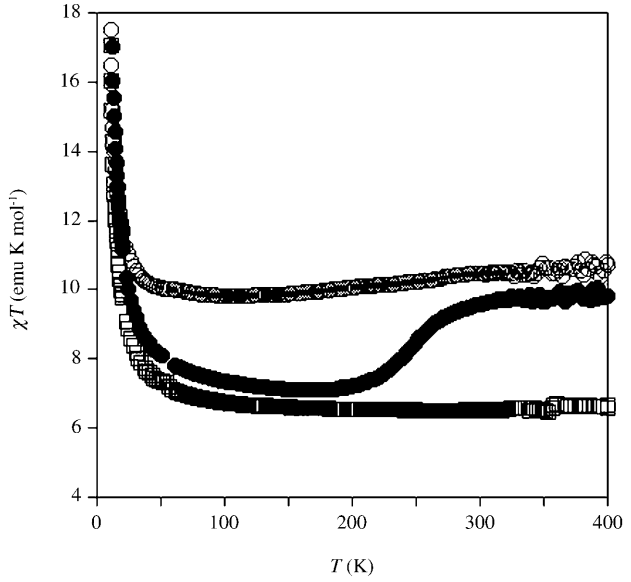

Figure 7. Temperature dependence of the product of the molar magnetic susceptibility with temperature (χT) at 0.1 T for compounds **1** (●), **2** (○), and **3** (□).

works.[2a,3] To confirm the presence of long-range magnetic ordering and to determine precisely the critical temperatures, alternating current (AC) susceptibility measurements were carried out. A maximum in the in-phase signal (χ') near T_c and an out-of-phase signal (χ'') that starts to appear at temperatures just below T_c is observed (Figure 8). From this data, the T_c of **1** is 5.4 K, similar to those reported for other Mn^{II}–Cr^{III} 2D oxalate compounds.[2a,3] These signals are frequency independent, as expected for a ferromagnet (Figure 8). In the ordered phase, an additional peak in χ'' at

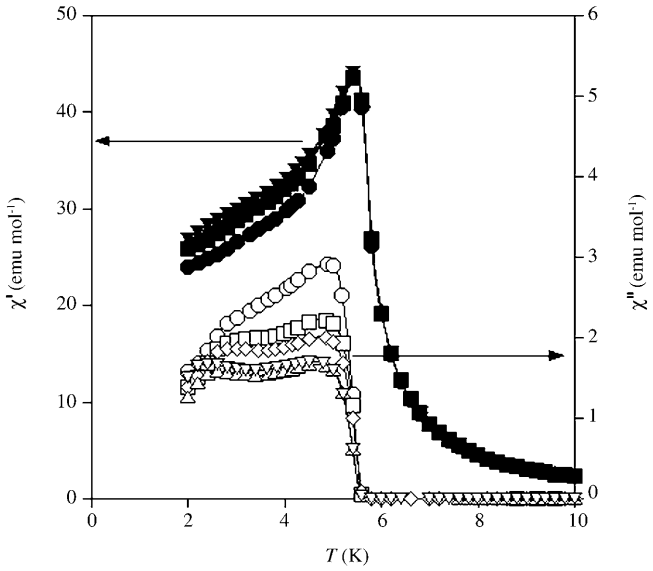

Figure 8. Temperature dependence of the in-phase AC susceptibility (χ') (filled symbols) and the out-of-phase AC susceptibility (χ'') (empty symbols) for **1**: ● 997 Hz, ■ 332 Hz, ◆ 110 Hz, ▲ 10 Hz, ▼ 1 Hz.

temperatures below 3 K is also detected. The presence of such a frequency-dependent peak has already been observed in other 2D M^{II}–Cr^{III} 2D oxalate compounds.[3] It can be related to the formation of magnetic domains and domain-wall movement.[19]

To confirm the ferromagnetic ordering of the spins, isothermal magnetization at 2 K was performed (Figure 9). It presented a sharp increase at low fields that is much faster than that expected for noninteracting Cr^{III} and Mn^{II} centers;

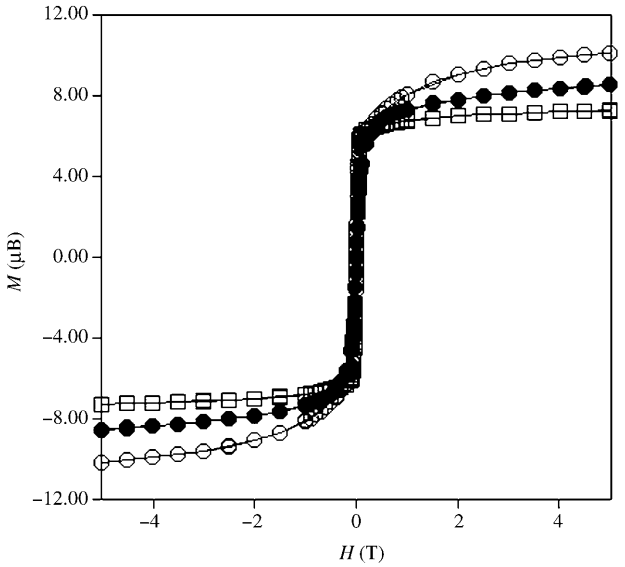

Figure 9. Field dependence of the magnetization (M) for **1** (●) **2** (○), and **3** (□).

this increase is more gradual at higher fields and no saturation is reached up to 5 T. The magnetization (M) value at 5 T is $8.5\mu_B$ (μ_B = Bohr magneton), which is slightly lower than the expected value for a parallel alignment of the spins in the bimetallic lattice ($9\mu_B$). It can be due to a spin canting of the ferromagnetic phase, as for other M^{II}–Cr^{III} 2D oxalate compounds.[3] The hysteresis loops at 2 K show that this compound is a soft ferromagnet with a coercive field of 2 mT.

The magnetic behavior of this compound after heating at 400 K under vacuum for 1 h has been studied because removal of solvent molecules may cause drastic changes in the spin-crossover behavior of this cation, as shown in other $[Fe(sal_2\text{-trien})]^+$ salts.[15,20] However, in contrast to similar compounds,[15] desolvation could not achieved, as microanalysis continued to show the presence of Cl in a 2:1 ratio with respect to Mn, Cr, and Fe.

Magnetic properties of 2 and 3: The thermal dependence of χT for **2** shows a value of 10.7 emu K mol^{-1} at 400 K (Figure 7). This value is close to the sum of the expected contributions for the isolated paramagnetic ions with 100% of Fe^{III} in a HS state. Furthermore, this value is 4.2 emu K mol^{-1} higher than that obtained for the reference

compound (**3**) with diamagnetic $[In(sal_2\text{-trien})]^+$ in the place of $[Fe(sal_2\text{-trien})]^+$. This confirms that $[Fe(sal_2\text{-trien})]^+$ is 100% HS at this temperature. χT presents a smooth decrease from 300 (10.5 emu K mol^{-1}) to 115 K (9.8 emu K mol^{-1}) as temperature decreases. The χT value of **2** at 300 K and the difference with that of **3** (4.0 emu K mol^{-1}) are consistent with the Mössbauer data that suggest that Fe^{III} is 93% HS at this temperature. On the other hand, the difference between χT values of **2** and **3** at 115 K is 3.1 emu K mol^{-1}, which is again consistent with the Mössbauer data that suggest that the fraction of LS Fe^{III} remains constant and close to 30% below 130 K. Therefore, the HS→LS spin conversion of 30% of the Fe^{III} complexes takes place between 300 and 130 K. This contrasts with the magnetic behavior of **1** that presents a complete spin conversion. At temperatures below 115 K there is an increase of χT, which is very sharp below 50 K. This indicates the presence of ferromagnetic interactions between neighboring Mn^{II}–Cr^{III} magnetic ions and the onset of long-range ferromagnetic ordering as usual for this type of compound. The χ^{-1} versus T curve of **3** is linear in the 50–300 K temperature range. This allows one to fit it to a Curie–Weiss law ($\chi^{-1}=(T-\theta)/C$, in which C is the Curie constant) and thus to a Weiss constant, θ, of 3.7 K, which is slightly lower than that obtained for a chiral 3D Mn^{II}–Cr^{III} oxalate network in the $[Ir(ppy)_2(bpy)][M^{II}Cr^{III}(ox)_3]\cdot 0.5H_2O$ compound (6.1 K).[11f] The long-range ferromagnetic ordering of the two compounds is confirmed by AC susceptibility measurements (see Figure 10) that show frequency-independent χ' and χ'' peaks. From this data, the T_c of compounds **2** and **3** is in both cases 5.2 K.

Isothermal magnetization at 2 K of the two compounds presents a sharp increase at low fields (below 0.1 T), and a hysteresis loop with a coercive field of approximately 3 mT, which is usual for this type of compound (Figure 9). In **3**, only the bimetallic oxalate sublattice is magnetic, so the magnetization tends to saturate and only a slight linear increase of M versus magnetic field (H) is observed at fields above 0.1 T as a consequence of spin canting in the ferromagnetic phase. In contrast, in **2**, the presence of a fraction of paramagnetic Fe^{III} produces a pronounced curvature in the M versus H curve with M increasing from 7.5 to 10μ_B when H increases from 0.1 to 5 T. In these two compounds, the difference between the M values at 5 T (ca. 3μ_B) is consistent with the presence of 70% of Fe^{III} in the HS state in **2**.

The magnetic behavior of **2** and **3** after desolvation has also been studied. In both cases, there are small differences with respect to the solvated sample. χT of the desolvated sample presents a more gradual decrease upon lowering the temperature, with values slightly higher than those of the initial sample from 300 to 100 K (see Figure 7SS in the Supporting Information). Thus, χT of the desolvated sample at 115 K is 0.3 emu K mol^{-1} higher than that of the solvated one. We could relate these differences to changes in the spin state of Fe^{III}. However, this is a very small effect that could be related also to structural changes in the oxalate network

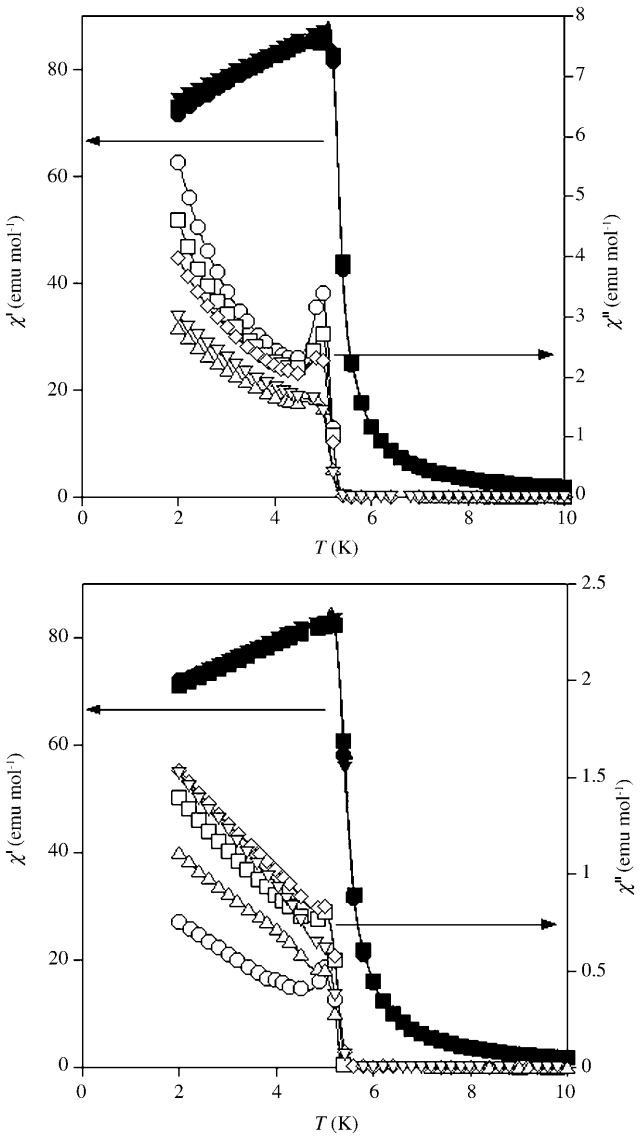

Figure 10. Temperature dependence of the in-phase AC susceptibility (χ') (filled symbols) and the out-of-phase AC susceptibility (χ'') (empty symbols) for **2** (top) and **3** (bottom): ● 997 Hz, ■ 332 Hz, ◆ 110 Hz, ▲ 10 Hz, ▼ 1 Hz.

(changes in distances and angles between the metallic centers). Thus, a slight increase of χT is also observed for the In^{III} analogoue, **3**, which does not contain a spin-crossover cation. Some differences appear also in AC susceptibility measurements of **2** and **3** with respect to the initial sample. Thus, both the χ' and χ'' peaks are shifted towards lower (T_c of 5.0 versus 5.2 K) temperatures and their intensity decreases with respect to the initial compound (see Figure 8SS in the Supporting Information). Again, these changes may be related to the oxalate network, as they occur in both compounds.

Magnetic properties of 4: χT of **4** presents a value of 6.5 emu K mol^{-1} at 300 K and an increase upon lowering the temperature, with a sharp increase below 50 K (Figure 9SS

in the Supporting Information). This confirms the ferromagnetic interaction between Mn^{II} and Cr^{III} ions of the oxalate network and the ferromagnetic behavior already observed in **2** and **3**. AC susceptibility measurements show a frequency-independent peak that starts to appear at 5.0 K and defines T_c (Figure 10SS in the Supporting Information). The isothermal magnetization at 2 K shows a very sharp increase at low fields and does not saturate completely at 5 T (see Figure 11SS in the Supporting Information). An M value of $7.8\mu_B$ is obtained at 5 T, as expected for a Mn^{II}–Cr^{III} ferromagnet. A hysteresis loop of the magnetization with a coercive field of 3 mT is observed at 2 K. All these features indicate that the ferromagnetic behavior of this 3D oxalate network is analogous to that of **3**. The slight decrease of T_c with respect to that of **2** and **3** may be explained by the slightly longer mean Mn^{II}–Cr^{III} distances shown by **4** (5.408 Å for **4** compared to 5.399 Å for **3**) and by slight differences in the bonding angles.

In any case, the T_c values obtained in the reported Mn^{II}–Cr^{III} 3D oxalate compound are all very close (5.2 K in **2** and **3**; 5.0 K in **4**) and similar to that shown by the chiral compound $[Ir(ppy)_2(bpy)][Mn^{II}Cr^{III}(ox)_3]\cdot 0.5\,H_2O$ (T_c = 5.1 K[11f]). Still, in the compound $[Fe(bpp)_2][MnCr(ox)_3]\cdot bpp\cdot CH_3OH$, which presents an achiral 3D oxalate network but longer Mn^{II}–Cr^{III} distances (5.503 Å), a significantly lower T_c value has been observed (T_c = 3.0 K).[14] It seems therefore that a correlation purely based on the Mn^{II}–Cr^{III} distances (longer for most of the chiral compounds) is not correct in this case, and other factors should also be involved. In this context we have demonstrated in a recent study that the decrease in T_c observed in the 3D series of bimetallic oxalates with respect to the 2D series can be explained by the noncollinear alignment of the chiral axis in the 3D compounds, as they produce differences in the relative orientation of the magnetic orbitals.[21] Hence, in an achiral 3D lattice, the T_c values should be intermediate between those shown by the 2D and the chiral 3D lattices if the distances between metals ions and other structural factors are kept similar. That is so because an achiral 3D lattice contains both homochiral (similar to those found in chiral 3D structures) and heterochiral (similar to those found in 2D structures) pairs of neighboring magnetic ions. Preliminary results in a chiral 3D analogue of **2** that exhibits a lower T_c value (4.8 K compared to 5.2 K in **2**) confirm this point.[22]

Mössbauer spectroscopy of 1: The Mössbauer spectrum of **1** obtained at 4 K shows only two well-defined peaks and may be fitted with a quadrupole doublet with isomer shift (IS) and quadrupole splitting (QS) typical of LS Fe^{III} (see Figure 11).[20a,23] Up to 160 K there is no change in the shape of the Mössbauer spectra. At 165 K, a very small absorption is observed between both peaks of the LS Fe^{III} doublet. This absorption increases as the temperature increases and may be fitted with two broad peaks with IS and QS typical for HS Fe^{III}.[20a,23] The coexistence of LS and HS Fe^{III} above 165 K, as well as the increase in the relative areas (I) of the

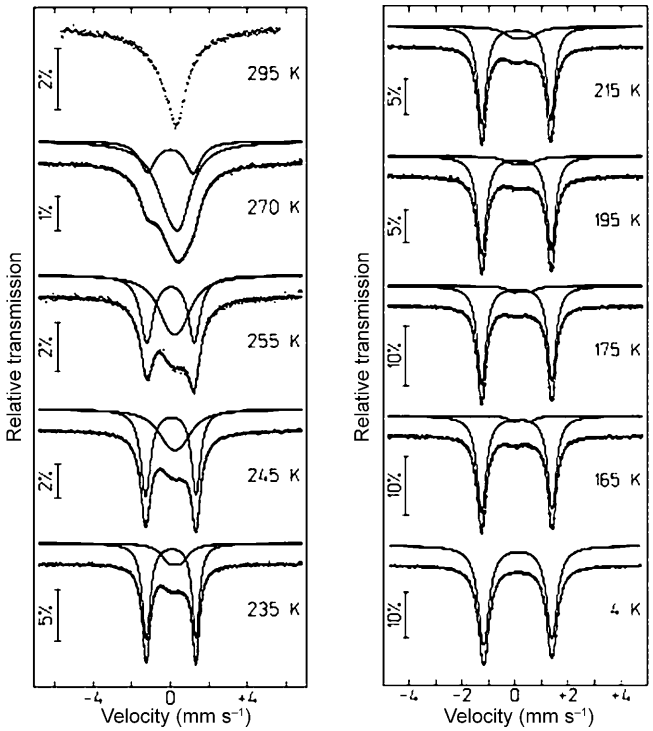

Figure 11. Mössbauer spectra of **1** taken at different temperatures. The lines over the experimental points are the sum of two doublets that correspond to HS and LS Fe^{III}. The estimated parameters for these doublets are collected in Table 1SS in the Supporting Information.

HS Fe^{III} with increasing temperature, agree with magnetization data.

The HS Fe^{III} absorption peaks significantly broaden with increasing temperature and above 235 K the same is observed for LS Fe^{III} peaks. At 255 K, the LS Fe^{III} peaks, although quite broad, are still resolved, but at 270 K and above this is no longer the case. Such behavior of the spectra may be understood if a dynamic $^2T\leftrightarrow{}^6A$ spin interconversion occurs and the spin-state lifetimes are comparable to the Mössbauer timescale, 10^{-7} s.[23c] Up to 255 K, since the HS and LS signals are distinct, we may infer that the spin-state interconversion rate is still slow relative to the Mössbauer timescale. At 270 K, signals for the HS and LS species strongly overlap, and at 295 K it is not possible to distinguish them, although magnetic susceptibility data indicate that an appreciable LS population is still present at this temperature.

The estimated HS Fe^{III} fractions from Mössbauer and magnetization data are in good agreement up to 270 K. Between 165 and 255 K, the LS fraction deduced from magnetic susceptibility is slightly lower than the corresponding relative areas (I) estimated from the Mössbauer spectra (see Table 1SS in the Supporting Information). There are many effects that may contribute to differences between the values estimated from both techniques. In general, due to the shorter and stronger Fe–ligand chemical bonds in the LS Fe^{III} molecules, the recoilless fraction of these Fe^{III} species is higher than that of the HS Fe^{III}, particularly above 80 K.

Consequently, the estimated I for LS Fe^{III} may be higher than the actual fraction. Broad peaks in the spectra of compound **1** also lead to higher uncertainties in the estimated I. Moreover, the fraction of HS Fe^{III} deduced from magnetic susceptibility data may be overestimated, particularly at lower temperatures, due to the ferromagnetic coupling between Mn^{II} and Cr^{III} neighbors. It should also be noted that the ferromagnetic ordering that occurs in the oxalate layer, detected by magnetization data, has no effect in the Mössbauer spectra. The LS Fe^{III} remain paramagnetic below T_c.

Mössbauer spectroscopy of 2: In the Mössbauer spectra of **2**, two contributions are observed in the temperature range 2.2–297 K (see Figure 12). One is a quadrupole doublet with

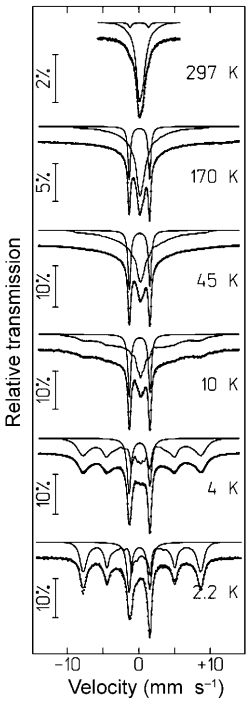

Figure 12. Mössbauer spectra of **2** taken at different temperatures. The lines over the experimental points are the sum of a doublet and a distribution of B_{hf} that corresponds to LS and HS Fe^{III}. The estimated parameters for these doublets are collected in Table 2SS in the Supporting Information.

estimated parameters typical of LS Fe^{III}. The other one consists of an unresolved absorption centered at IS≈0.34 (297 K)–0.45 mm s^{-1} (4 K). This contribution gradually broadens as the temperature decreases. At 10 K, the maxima of four peaks belonging to a sextet appears on the absorption band. This sextet is clearly observed at 4 K with an estimated magnetic hyperfine field B_{hf}≈51 T; the corresponding peaks sharpen down to 2.2 K (B_{hf}≈52 T). The estimated IS and B_{hf} for this contribution are typical of HS Fe^{III}.

Broadening of the HS Fe^{III} peaks was also observed in $[Fe(acac)_2trien]BPh_4$ and $[Fe(acac)_2trien]PF_6$[23a] (acac = acetylacetonate), and has been attributed to dynamic effects during the timescale 10^{-6}–10^{-8} s, the order of magnitude of the lifetime of the Mössbauer excited nuclear state.[23] These effects may be either related to the lifetimes of the electronic $S=1/2$ and $S=5/2$ states in the temperature range in which both states coexist, or to fluctuations of the directions of the Fe magnetic moments, μ_{Fe}, with a frequency along the order of 10^7 s^{-1}. When the spin-state interconversion between the HS and LS states is comparable or faster than the reciprocal of the Mössbauer time window, the corresponding doublets are expected to fuse into a single one with increasing temperature,[23c] as observed for compound **1**. Since both LS and HS Fe^{III} contributions are separately observed in the spectra of compound **2**, the fluctuations between spin states (frequencies $<10^7$ s^{-1}) are slow compared to the Mössbauer timescale at all measured temperatures. Therefore the HS Fe^{III} absorption broadening is only related to slow fluctuations of the magnetic hyperfine interaction caused by the slow relaxation of μ_{Fe} directions.

A sextet is observed when the frequency of fluctuation of the μ_{Fe} directions is lower than 10^7 s^{-1}.[24] This is the case when μ_{Fe} are magnetically ordered. However, such low frequencies may also be observed in the case of paramagnetic Fe atoms with slow μ_{Fe} relaxation. For compound **2**, one should be cautious since no sudden freezing of the μ_{Fe} in the $[Fe(sal_2\text{-trien})]^+$ occurs at the magnetic-ordering temperature of the $[MnCr(ox)_3]$ layers. Instead, a slow paramagnetic relaxation frequency of 10^7–10^9 s^{-1} is already observed at 170 K and it slows down gradually as the temperature decreases. Furthermore, no effect of the ferromagnetic ordering is observed in the LS Fe^{III} contribution, as in the case of compound **1**.

The LS Fe^{III} contributions to the spectra are well-defined quadrupole doublets within the 297–2.2 K temperature range. This means that, as usual, slow relaxation of μ_{Fe} is only observed for HS Fe^{III} and not for LS Fe^{III}. In fact, HS Fe^{III}, in the electronic ^6S state, is characterized by vanishing orbital momentum. The only relaxation mechanism available in this case is spin–spin (i.e., energy transfer may only occur between interacting spins). A sizeable orbital moment is, however, expected for LS Fe^{III}, and the corresponding spins may interact by means of spin–orbit and orbital–phonon coupling with the phonons, the so-called spin-lattice relaxation mechanism. This mechanism explains why μ_{Fe} relaxation is fast for LS Fe^{III}. By simulating the broad absorption of HS Fe^{III} with the distribution of B_{hf}, the estimated relative areas (Table 2SS in the Supporting Information) suggest that the fraction of HS Fe^{III} drops from around 93% at 297 K to around 72% at 130 K. Below this temperature, it remains approximately constant (≈70%) down to 2.2 K. At 4 and 2.2 K, the distribution of B_{hf} narrows significantly and, as mentioned above, is centered at B_{hf}≈51 and 52 T, respectively.

Conclusion

We have reported in this paper the first examples of molecular materials with coexistence of ferromagnetism and spin crossover. The materials are salts formed by the insertion of a spin-crossover Fe^{III} cation complex into anionic coordination polymers based on bimetallic oxalate complexes. From the chemical point of view, we have shown that the use of different mixed solvents and the same templating cation, which can adopt a variable configuration in the crystalline lattice, is a suitable strategy to obtain different oxalate networks. Thus, by changing the experimental conditions, two different oxalate networks, a 2D structure in compound **1** and an unusual achiral 3D structure in compounds **2**, **3**, and **4**, have been obtained with the same templating cation, $[Fe(sal_2\text{-trien})]^+$.

From the point of view of the physical properties, we have found that the magnetic properties and the Mössbauer spectroscopy of **1** indicate the coexistence of an almost complete spin crossover of 100% of Fe^{III} ions from 300 to 160 K, and a ferromagnetic ordering below 5.4 K in the layered magnet. In turn, **2** shows a gradual spin-crossover of 30% of the Fe^{III} from 300 to 130 K, together with a ferromagnetic ordering in the 3D lattice below 5.2 K. The preparation of the reference compounds **3** and **4** have allowed us to study the magnetic properties of the 3D lattice alone. They have shown that, in this case, the spin-crossover phenomenon does not influence the magnetic ordering. On the other hand, the magnetic properties of **2**, **3**, and **4** indicate that the ordering temperature of this achiral 3D network, T_c, is slightly higher than those observed in the chiral 3D analogues.

A very promising possibility provided by this hybrid strategy is to tune the magnetic ordering of the $Mn^{II}Cr^{III}$ oxalate network, thereby inducing the spin crossover of the intercalated spin-crossover cations by applying light or pressure. Compound **1** seems a better candidate for this purpose as it undergoes a complete spin-crossover; however, it is unexpected that the changes in the structure of the intercalated compound could modify the T_c of the 2D oxalate network, as 2D oxalate networks with different interlayer separations present similar T_c values. In fact, the spin-crossover transition can be seen as an internal anisotropic pressure that may induce small structural changes in the ferromagnetic sublattice. In this sense, compound **2**, which is formed by a 3D magnetic network, is expected to be much more sensitive to the influence of this internal pressure. Unfortunately, in this case the HS state is highly favored; therefore, the occurrence of a spin crossover and its influence on the ferromagnetic sublattice is very limited.

We can conclude that hybrid magnets with coexistence of magnetic ordering and spin crossover can be designed using this molecular approach. Although the preparation of hybrid switchable magnets has not yet been reached, the synthetic strategy presented in this paper opens the way to the preparation of these new type of magnets. Apart from this final goal, the versatility of this method to combine two molecular subnetworks in the same compound could give rise to new physical properties that stem from this unusual combination. This has been achieved in one of the compounds presented in this paper. Thus, in the ordered ferromagnetic state (below 5 K), the Mössbauer spectrum of **2** has shown the appearance of a sextet associated with HS Fe^{III}. However, this new phenomenon in $[Fe(sal_2\text{-trien})]^+$ compounds, the slow relaxation of the magnetic moment of HS Fe^{III}, is also observed at temperatures much higher than the magnetic ordering of the oxalate network. There is therefore no clear evidence of a relation between both phenomena.

Experimental Section

Synthesis: The complexes $[Fe(sal_2\text{-trien})]PF_6$ and $[In(sal_2\text{-trien})]PF_6$ were prepared according to literature methods.[23a] $Ag_3[Cr(ox)_3]$ was prepared by metathesis from the corresponding potassium salt.[25] All other materials and solvents were commercially available and used without further purification.

Compound 1: Crystals of this compound were obtained by slow diffusion of two solutions. The first solution was prepared by adding $MnCl_2{\cdot}4H_2O$ (0.053 g, 0.268 mmol) to a suspension of $Ag_3[Cr(ox)_3]$ (0.114 g, 0.179 mmol) in methanol (8 mL). The AgCl precipitate was filtered. The second solution was obtained by dissolving $[Fe(sal_2\text{-trien})]PF_6$ (0.100 g, 0.179 mmol) in dichloromethane (8 mL). After two weeks, brown crystals were obtained.

Compound 2: Crystals of this compound were obtained by slow diffusion of two solutions. The first solution was prepared by adding $MnCl_2{\cdot}4H_2O$ (0.053 g, 0.268 mmol) to a suspension of $Ag_3[Cr(ox)_3]$ (0.114 g, 0.179 mmol) in methanol (7 mL). The AgCl precipitate was filtered. The second solution was obtained by dissolving $[Fe(sal_2\text{-trien})]PF_6$ (0.100 g, 0.179 mmol) in acetonitrile (7 mL). After two weeks, brown crystals were obtained.

Compound 3: Crystals of this compound were obtained by slow diffusion of two solutions. The first solution was prepared by adding $MnCl_2{\cdot}4H_2O$ (0.053 g, 0.268 mmol) to a suspension of $Ag_3[Cr(ox)_3]$ (0.114 g, 0.179 mmol) in methanol (8 mL). The AgCl precipitate was filtered. The second solution was obtained by dissolving $[In(sal_2\text{-trien})]PF_6$ (0.110 g, 0.179 mmol) in acetonitrile (8 mL). After three weeks, violet crystals were obtained.

Compound 4: Crystals of this compound were obtained by slow diffusion of two solutions. The first solution was prepared by adding $MnCl_2{\cdot}4H_2O$ (0.072 g, 0.364 mmol) to a suspension of $Ag_3[Cr(ox)_3]$ (0.155 g, 0.242 mmol) in methanol (12 mL). The AgCl precipitate was filtered. The second solution was prepared by dissolving $[In(sal_2\text{-trien})]PF_6$ (0.150 g, 0.242 mmol) in nitromethane (12 mL). After three weeks, violet crystals were obtained.

Structural characterization: Single crystal X-ray data were collected at 180 K for compound **1**, 120 K for compound **2**, and 150 K for compounds **3** and **4** by using a Nonius KappaCCD diffractometer equipped with graphite-monochromated $Mo_{K\alpha}$ radiation ($\lambda = 0.71073$ Å). The Denzo and Scalepack programs were used for cell refinements and data reduction of the four compounds.[26] Crystal structures were solved by direct methods using the SIR97 program,[27] and refined against all F^2 values using the SHELXL-97 program.[28] Non-hydrogen atoms were refined anisotropically (except as noted); hydrogen atoms were placed in calculated positions that were refined using idealized geometries (riding model) and assigned fixed isotropic displacement parameters. In **3**, one of the two crystallographically independent sal_2-trien ligands was modeled in two orientations in a 59.7(10):40.3(10) ratio. Carbon, nitrogen, and oxygen atoms of some of the sal_2-trien ligands could only be modeled isotropically for compounds **2** and **3**, possibly due to the flexibility

Table 1. Crystallographic data for compounds **1**, **2**, **3**, and **4**.

Compound	**1**	**2**	**3**	**4**
formula	$C_{27}H_{26}Cl_2CrFeMnN_4O_{14}$	$C_{54}H_{56}Cr_2Fe_2Mn_2N_8O_{30}$	$C_{53.5}H_{52.5}Cr_2In_2Mn_2N_{8.5}O_{29}$	$C_{54}H_{48}Cr_2In_2Mn_2N_{10}O_{33}$
M_r	864.2065	1622.6329	1722.0495	1808.5270
crystal color	brown	brown	violet	violet
T [K]	180	120	150	150
crystal system	monoclinic	monoclinic	monoclinic	orthorhombic
Z	4	4	4	4
space group	$P2_1/c$	Cc	Cc	$Pna2_1$
a [Å]	11.6440(2)	21.9180(9)	21.5690(7)	20.4650(3)
b [Å]	31.7710(5)	14.0330(9)	14.1590(7)	21.2430(5)
c [Å]	9.5340(3)	22.4670(15)	22.7360(9)	16.2740(5)
β [°]	110.2370(11)	92.639(4)	91.116(2)	90
V [Å^3]	3309.30(13)	6903.0(7)	6942.2(5)	7074.9(3)
ρ_{calcd} [Mg m^{-3}]	1.735	1.561	1.659	1.698
$\mu(Mo_{K\alpha})$ [mm^{-1}]	1.367	1.157	1.405	1.378
θ range [°]	1.28 to 27.48	1.72 to 21.77	1.72 to 27.45	1.38 to 27.49
reflns collected	13485	8013	12959	15664
independent reflns (R_{int})	7451 (0.0471)	8006 (0.0273)	12955 (0.0617)	15664 (0.1364)
LS params/restraints	475/0	671/2	790/36	790/1
$R1(F)$[a] ($I>2\sigma(I)$)	0.0557	0.0798	0.0710	0.0621
$wR2(F^2)$[b] (all data)	0.1519	0.1435	0.1440	0.1120
$S(F^2)$[c] (all data)	1.116	1.017	0.970	1.033

[a] $R1(F)=S(|F_o|-|F_c|)/S|F_o|$. [b] $wR2(F^2)=[Sw(F_o^2-F_c^2)^2/SwF_o^4]^{1/2}$. [c] $S(F^2)=[Sw(F_o^2-F_c^2)^2/(n-p)]^{1/2}$.

of the ligand. The use of restraints and/or constraints in the refinement of the structures is documented in the corresponding CIFs. Data collection and refinement statistics are collected in Table 1. CCDC-749068 (**1**), -749069 (**2**), -749070 (**3**), and -749071 (**4**) contain the supplementary crystallographic data for this paper. These data can be obtained free of charge from The Cambridge Crystallographic Data Centre via www.ccdc.cam.ac.uk/data_request/cif.

Physical measurements: Magnetic susceptibility measurements were performed on polycrystalline samples by using a magnetometer (Quantum Design MPMS-XL-5) equipped with a SQUID sensor. Variable-temperature measurements were carried out in the temperature range 2–400 K. The AC measurements were performed in the temperature range 2–10 K at different frequencies with an oscillating magnetic field of 0.395 mT. The magnetization and hysteresis studies were performed between 5 and −5 T and by cooling the samples at zero field. The Fe/Mn/Cr/Cl and In/Mn/Cr ratios were measured using a Philips ESEM X230 scanning electron microscope equipped with an EDAX DX-4 microsonde. Mössbauer spectra were collected in transmission mode using a conventional constant-acceleration spectrometer and a 25 mCi ^{57}Co source in an Rh matrix. The velocity scale was calibrated using α-Fe foil. The absorber was obtained by pressing powdered single crystals of **1** or **2** into a Perspex holder. Low-temperature spectra were collected using a bath cryostat with the sample immersed in liquid He for measurements at 4.1 and 2.2 K, or by using flowing He gas to cool the sample above 4.1 K (temperature stability of 0.2 K). The spectra were fitted to Lorentzian lines using a nonlinear least-squares method.[29] Isomer shifts (Tables 1SS and 2SS in the Supporting Information) are given relative to metallic α-Fe at room temperature.

Acknowledgements

Financial support from the European Union (MolSpinQIP and SPINMOL ERC Advanced Grant), the Spanish Ministerio de Ciencia e Innovación (Project Consolider-Ingenio in Molecular Nanoscience, CSD2007-00010, and projects CTQ2005-09385-C03 and MAT2007-61584), and the Generalitat Valenciana (Prometeo Program) are gratefully acknowledged. The authors also thank J. M. Martínez-Agudo of the University of Valencia for assistance with the preparation and magnetic characterization of the samples.

[1] a) E. Coronado, P. Day, *Chem. Rev.* **2004**, *104*, 5419; b) E. Coronado, J. R. Galán-Mascarós, *J. Mater. Chem.* **2005**, *15*, 66.
[2] a) H. Tamaki, Z. J. Zhong, N. Matsumoto, S. Kida, M. Koikawa, N. Achiwa, Y. Hashimoto, H. Okawa, *J. Am. Chem. Soc.* **1992**, *114*, 6974; b) H. Tamaki, M. Mitsumi, N. Nakamura, N. Matsumoto, S. Kida, H. Okawa, S. Ijima, *Chem. Lett.* **1992**, 1975; c) C. Mathonière, S. G. Carling, D. Yuscheng, P. Day, *J. Chem. Soc. Chem. Commun.* **1994**, 1551; d) C. Mathonière, J. Nutall, S. G. Carling, P. Day, *Inorg. Chem.* **1996**, *35*, 1201; e) R. Pellaux, H. W. Schmalle, R. Huber, P. Fisher, T. Hauss, B. Ouladdiaf, S. Decurtins, *Inorg. Chem.* **1997**, *36*, 2301; f) E. Coronado, J. R. Galán-Mascarós, C. J. Gómez-García, J. M. Martínez-Agudo, E. Martínez-Ferrero, J. C. Waerenborgh, M. Almeida, *J. Solid State Chem.* **2001**, *159*, 391; g) K. S. Min, A. L. Rhinegold, J. S. Miller, *Inorg. Chem.* **2005**, *44*, 8433; h) E. Coronado, J. R. Galán-Mascarós, C. Martí-Gastaldo, *J. Mater. Chem.* **2006**, *16*, 2685.
[3] a) M. Clemente-León, J. R. Galán-Mascarós, C. J. Gómez-García, *Chem. Commun.* **1997**, 1727; b) E. Coronado, J. R. Galán-Mascarós, C. J. Gómez-García, J. M. Martínez-Agudo, *Adv. Mater.* **1999**, *11*, 558; c) E. Coronado, J. R. Galán-Mascarós, C. J. Gómez-García, J. Ensling, P. Gutlich, *Chem. Eur. J.* **2000**, *6*, 552.
[4] E. Coronado, C. Giménez-Saiz, C. J. Gómez-Garcia, F. M. Romero, A. Tarazón, *J. Mater. Chem.* **2008**, *18*, 929.
[5] a) S. Bénard, P. Yu, J. P. Audière, E. Rivière, R. Clèment, J. Ghilhem, L. Tchertanov, K. Nakatami, *J. Am. Chem. Soc.* **2000**, *122*, 9444; b) S. M. Aldoshin, N. A. Sanina, V. I. Minkin, N. A. Voloshin, V. N. Ikorskii, V. I. Ovcharenko, V. A. Smirnov, N. K. Nagaeva, *J. Mol. Struct.* **2007**, *826*, 69.
[6] S. Bénard, E. Rivière, P. Yu, K. Nakatami, J. F. Delouis, *Chem. Mater.* **2001**, *13*, 159.
[7] a) E. Coronado, J. R. Galán-Mascarós, C. J. Gómez-García V. Laukhin, *Nature* **2000**, *408*, 447; b) A. Alberola, E. Coronado, J. R. Galán-Mascarós, C. Giménez-Saiz, C. J. Gómez-García, *J. Am. Chem. Soc.* **2003**, *125*, 10774; c) E. Coronado, J. R. Galán-Mascarós, C. J. Gómez-García, E. Martínez-Ferrero, S. Van Smaalen, *Inorg. Chem.* **2004**, *43*, 4808.
[8] M. Clemente-León, E. Coronado, J. C. Dias, A. Soriano-Portillo, R. D. Willett, *Inorg. Chem.* **2008**, *47*, 6458.
[9] C. Train, R. Gheorghei, V. Krstic, L. M. Chamoreau, N. S. Ovanesyan, G. L. J. A. Rikken, M. Gruselle, M. Verdaguer, *Nat. Mater.* **2008**, *7*, 729.

[10] a) F. D. Rochon, R. Melanson, M. Andruh, *Inorg. Chem.* **1996**, *35*, 6086; b) M. Andruh, R. Melanson, C. V. Stager, F. D. Rochon, *Inorg. Chim. Acta* **1996**, *251*, 309; c) N. Stanica, C. V. Stager, M. Cimpoesu, M. Andruh, *Polyhedron* **1998**, *17*, 1787; d) G. Marinescu, M. Andruh, R. Lescouëzec, M. C. Muñoz, J. Cano, F. Lloret, M. Julve, *New J. Chem.* **2000**, *24*, 527; e) S. Triki, F. Berezovsky, J. S. Pala, E. Coronado, C. J. Gómez-García, J. M. Clemente, A. Riou, P. Molinie, *Inorg. Chem.* **2000**, *39*, 3771; f) G. Ballester, E. Coronado, C. Giménez-Saiz, F. M. Romero, *Angew. Chem.* **2001**, *113*, 814; *Angew. Chem. Int. Ed.* **2001**, *40*, 792; g) E. Coronado, C. Giménez-Saiz, J. R. Galán-Mascarós, C. J. Gómez-García, C. Ruiz-Pérez, *Eur. J. Inorg. Chem.* **2003**, 2290; h) E. Coronado, J. R. Galán-Mascarós, C. J. Gómez-García, C. Martí-Gastaldo, *Inorg. Chem.* **2005**, *44*, 6179; i) E. Coronado, J. R. Galán-Mascarós, C. Martí-Gastaldo, *Inorg. Chem.* **2006**, *45*, 1882; j) E. Coronado, J. R. Galán-Mascarós, C. Martí-Gastaldo, A. Murcia-Martínez, *Dalton Trans.* **2006**, 3294; k) H. Z. Kou, O. Sato, *Inorg. Chem.* **2007**, *46*, 9513; l) E. Cariati, R. Macchi, D. Roberto, R. Ugo, S. Galli, N. Casati, P. Macchi, A. Sironi, L. Bogani, A. Caneschi, D. Gatteschi, *J. Am. Chem. Soc.* **2007**, *129*, 9410; m) H. Z. Kou, J. Tao, O. Sato, *Dalton Trans.* **2008**, 3652.

[11] a) S. Decurtins, H. W. Schmalle, P. Schneuwly, H. R. Oswald, *Inorg. Chem.* **1993**, *32*, 1888; b) S. Decurtins, H. W. Schmalle, P. Schneuwly, J. Ensling, P. Gütlich, *J. Am. Chem. Soc.* **1994**, *116*, 9521; c) M. Hernández-Molina, F. Lloret, C. Ruiz-Pérez, M. Julve, *Inorg. Chem.* **1998**, *37*, 4141; d) E. Coronado, J. R. Galán-Mascarós, C. J. Gómez-García, J. M. Martínez-Agudo, *Inorg. Chem.* **2001**, *40*, 113; e) F. Pointillart, C. Train, M. Gruselle, F. Villain, H. W. Schmalle, D. Talbot, P. Gredin, S. Decurtins, M. Verdaguer, *Chem. Mater.* **2004**, *16*, 832; f) M. Clemente-León, E. Coronado, C. J. Gómez-García, A. Soriano-Portillo, *Inorg. Chem.* **2006**, *45*, 5653.

[12] a) R. Andrés, M. Gruselle, B. Malézieux, M. Verdaguer, J. Vaissermann, *Inorg. Chem.* **1999**, *38*, 4637; b) R. Andrés, M. Brissard, M. Gruselle, C. Train, J. Vaissermann, B. Malézieux, J. P. Jamet, M. Verdaguer, *Inorg. Chem.* **2001**, *40*, 4633.

[13] R. Sieber, S. Decurtins, H. Stoeckli-Evans, C. Wilson, D. Yufit, J. A. K. Howard, S. C. Capelli, A. Hauser, *Chem. Eur. J.* **2000**, *6*, 361.

[14] E. Coronado, J. R. Galán-Mascarós, M. C. Giménez-López, M. Almeida, J. C. Waerenborgh, *Polyhedron* **2007**, *26*, 1838.

[15] M. Clemente-León, E. Coronado, M. C. Giménez-López, A. Soriano-Portillo, J. C. Waerenborgh, F. S. Delgado, C. Ruiz-Pérez, *Inorg. Chem.* **2008**, *47*, 9111.

[16] C. Janiak, *J. Chem. Soc. Dalton Trans.* **2000**, 3885.

[17] R. Pritchard, S. A. Barrett, C. A. Kilner, M. A. Halcrow, *Dalton Trans.* **2008**, 3159.

[18] A. Alberola, E. Coronado, C. Giménez-Saiz, C. J. Gómez-García, F. M. Romero, A. Tarazón, *Eur. J. Inorg. Chem.* **2005**, 389.

[19] N. A. Chernova, Y. Song, P. Y. Zavalij, M. S. Wittingham, *Phys. Rev. B* **2004**, *70*, 144405.

[20] a) S. Floquet, S. Salunke, M. L. Boillot, R. Clément, F. Varret, K. Boukheddaden, E. Rivière, *Chem. Mater.* **2002**, *14*, 4164–4171; b) S. Floquet, M. C. Muñoz, E. Rivière, R. Clément, J. P. Audière, M. L. Boillot, *New J. Chem.* **2004**, *28*, 535.

[21] R. S. Fishman, M. Clemente-León, E. Coronado, *Inorg. Chem.* **2009**, *48*, 3039.

[22] Unpublished results.

[23] a) E. Sinn, G. Sim, E. V. Dose, M. F. Tweedle, L. J. Wilson, *J. Am. Chem. Soc.* **1978**, *100*, 3375; b) Y. Maeda, N. Tsutsumi Y. Takashima, *Inorg. Chem.* **1984**, *23*, 2440; c) M. Nihei, T. Shiga, Y. Maeda, H. Oshio, *Coord. Chem. Rev.* **2007**, *251*, 2606.

[24] N. N. Greenwood, T. C. Gibb, *Mossbauer Spectroscopy*, Chapman and Hall, London, **1971**, pp. 72–75.

[25] J. C. Baylar, E. M. Jones, *Inorganic Synthesis, Vol. 5* (Ed.: H. S. Booth), McGraw-Hill, New York, **1939**, p. 35.

[26] Z. Otwinowski, W. Minor, *Methods in Enzymology, Vol. 276* (Ed.: C. W. Carter, Jr., R. M. Sweet), Academic Press, New York, **1997**, p. 307.

[27] A. Altomare, M. C. Burla, M. Camalli, G. L. Cascarano, C. Giacovazzo, A. Guagliardi, A. G. G. Moliterni, G. Polidori, R. Spagna, *J. Appl. Crystallogr.* **1999**, *32*, 115–119.

[28] SHELXL-97: G. M. Sheldrick, University of Göttingen, Göttingen, **1997**.

[29] J. C. Waerenborgh, M. O. Figueiredo, J. M. P. Cabral, L. C. Pereira, *J. Solid State Chem.* **1994**, *111*, 300–309.

Received: September 28, 2009
Published online: December 28, 2009

